PCCP

ROYAL SOCIETY OF CHEMISTRY

REVIEW

View Article Online
View Journal | View Issue

Cite this: *Phys. Chem. Chem. Phys.*, 2025, **27**, 22871

Infrared spectroscopy at the surface of carbonates

Taha Elgayyar, * Federico Azzolina-Jury and Frédéric Thibault-Starzyk

Received 10th June 2025,
Accepted 2nd October 2025

DOI: 10.1039/d5cp02197a

rsc.li/pccp

IR spectroscopy has been extensively employed to characterize the structural and vibrational properties of carbonates; yet, its application in studying the adsorption capacity of carbonate surfaces remains limited. This short review presents the use of FTIR as a powerful tool for investigating the structure and surface chemistry of carbonates, which is relevant to several environmental and industrial applications (such as CO_2 capture and storage). Several FTIR techniques provide detailed analysis of the structure of carbonate polymorphs (calcite, aragonite, vaterite, and amorphous phases) alongside their phase transformation kinetics. In addition, adsorption studies of various molecules (CO, CO_2, H_2O, acids and several HCs) were performed to identify the adsorption sites, mechanisms and intermediates. These insights highlight the significance of IR spectroscopy for understanding the carbonate structure and surface properties, and guide future research in several environmental and industrial processes where carbonates are involved.

Introduction

The surface chemistry of solid carbonates has recently gained particular interest in the fight against the greenhouse effect and climate global warming, for CO_2 capture and storage, as well as for its further use (*e.g.* in methanation reactions[6]). Carbonates are also increasingly considered as adsorbent materials for various chemicals such CO,[1] H_2O,[1] CO_2[2] and HCs.[3–5]

Mastering surface chemistry of carbonates is not possible without a good understanding of the possible adsorption modes and of the various possible reaction mechanisms on the surface of carbonates. One of the most powerful methods for monitoring adsorption phenomena is infrared spectroscopy[6] and it has been used extensively to study the formation of surface carbonates by adsorption of CO_2 on various oxides.[7] Carbonates themselves have been studied by IR spectroscopy but a systematic study of adsorbed species on solid carbonates is still missing.

This work reviews literature information and data obtained by IR spectroscopy on the various chemical species found on the surface of carbonates, together with the basic information on the carbonate structure where relevant.

The infrared spectrum of the core structure of carbonates

Before it was used to study adsorbed species on carbonates, IR was largely employed in all spectral regions, from near to far IR, for characterising the composition, structure and crystalline phases of carbonates.

Vibration bands of the structure of the carbonate ion

Isolated planar ions of the form XO_3 with trigonal symmetry such as CO_3^{2-} exhibit four fundamental modes of vibration.[8,9] The frequencies of these vibration modes, as reported in the literature,[10,11] are shown in Table 1. An interesting feature is the progressive increase of the frequency of the $\nu 4$ vibration with the radius of the counter cations.[12]

Carbonates also display, between 2900 and 4000 cm^{-1}, some other IR absorption bands due to overtones and combinations of the fundamental bands,[13] including some weak combination bands at 1795 and 2514 cm^{-1}.[3] Interestingly, for studying surface species, some combination bands around 3000 cm^{-1}, indeed due to the carbonate structure, are sometimes mistaken for C–H stretch absorption bands.

The different IR techniques such as IRRAS, DRIFTS, transmission IR and ATR display differences in the spectra measured for the same sample. Fig. 1 (ref. 14) shows IR spectra of $BaCO_3$ measured using four IR techniques. This figure shows the higher surface sensitivity of DRIFTS and transmission IR as evidenced by the surface bands observed in the 2400–3000 cm^{-1} region and assigned to O–H stretching of hydrogen carbonate species,[15] while ATR and IRRAS are rather bulk-sensitive. Interestingly, there are noticeable band $\nu 3$ position shifts between all four techniques, mostly due to the instrument configuration. The IRRAS spectrum displayed a significant blueshift, which could be due to a change in the refractive index while scanning over the band range.

Université de Caen Normandie, ENSICAEN, CNRS, Laboratoire Catalyse et Spectrochimie, 14000 Caen, France. E-mail: tahaelgayyar1@gmail.com

Table 1 Approximate IR frequency ranges of the four fundamental vibration modes of carbonate[10,11]

Vibration mode	$\nu1$	$\nu2$	$\nu3$	$\nu4$
Assignment	Symmetric in-plane stretch	Out-of-plane bend	Asymmetric in-plane stretch	In-plane bend
Wavenumber (cm^{-1})	1070–1090	850–880	1400–1500	700–750

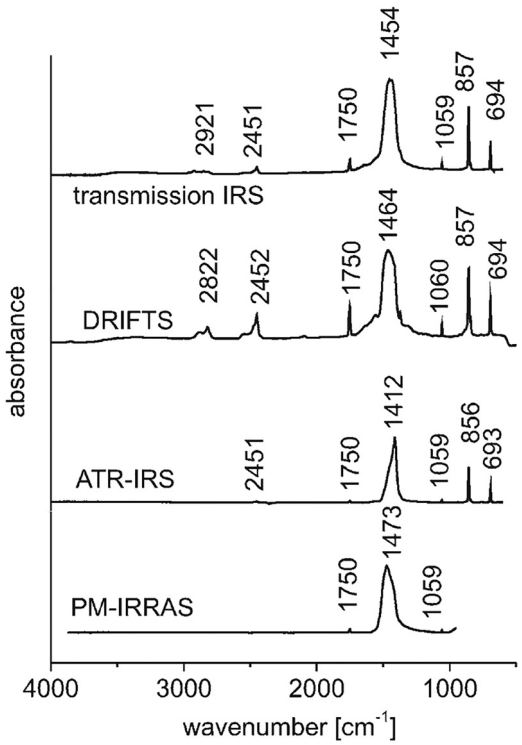

Fig. 1 IR spectra of $BaCO_3$ measured using different IR techniques. Adapted from ref. 14 with permission from Royal Society of Chemistry, copyright 2008.

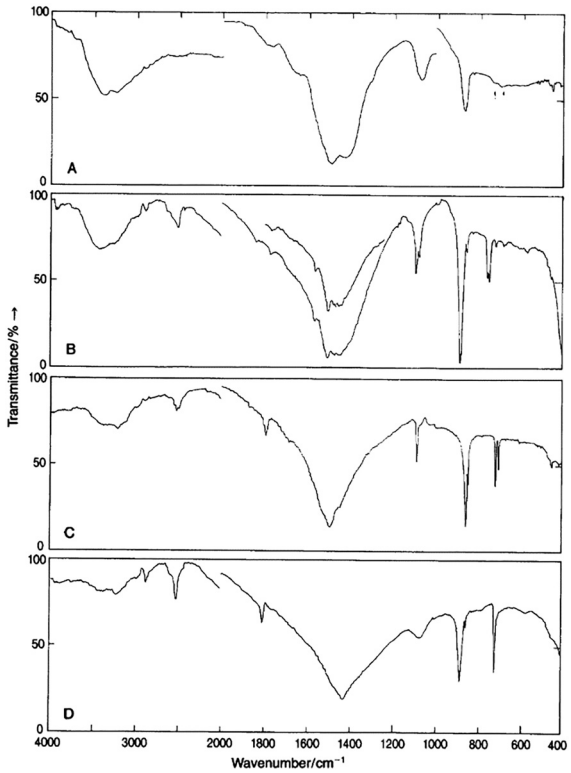

Fig. 2 IR spectra of (A) amorphous $CaCO_3$, (B) vaterite, (C) aragonite, and (D) calcite. Adapted from ref. 18 with permission from Scandinavian Society of Chemistry, copyright 1991.

Identification of crystalline phases in calcium carbonate

Calcium carbonate is the most abundant natural carbonate. It amounts for 4% of Earth's crust[16] and is the main component in chalk, a coral skeleton, and limestone.

IR spectroscopy provides information on the structure and properties of $CaCO_3$ polymorphs,[17–19] as displayed in Fig. 2.[18] The relative intensities of the $\nu1$ ($\sim$1100 cm^{-1}) and $\nu4$ ($\sim$700 cm^{-1}) and the splitting of the $\nu4$ and $\nu3$ (1400–1500 cm^{-1}) can be used to identify the varieties (amorphous $CaCO_3$, vaterite, aragonite or calcite), especially with noticeable low intensity of the $\nu1$ vibration band for calcite.

In the near-IR, several absorption bands are present due to overtones and combinations of the fundamental bands. The spectral region between 3920 and 28 600 cm^{-1} (Fig. 3) was used to identify and distinguish calcite, aragonite and dolomite using seven characteristic bands for carbonates in the range of 3900–6250 cm^{-1},[20] with major bands at 4000 cm^{-1} (ref. 21) and 4250–4350 cm^{-1}.[13,21]

Spectral features in the near IR and higher end of the MIR were used to determine carbonate content in arid soil samples.[22] However, the PLSR (partial least-squares regression) efficiency of the method was found to be only 52% due to the overlapping of other soil components (illite and chlorite) with similar spectral features. The accuracy would have been improved by extending the measurement range to lower frequency MIR and FIR.

Similarly, the spectral range 28 600–2000 cm^{-1} was used to detect anhydrous carbonate minerals using bands at $\sim$4350, 4000, 2940, 2560 and 2130 cm^{-1} (Fig. 4).[21] In addition, water related spectral features were detected at 10 000, 8330, 7140–6670, 5260, and 3570 cm^{-1}. However, some typical characteristic carbonate IR bands were shifted, weak or absent in the case of hydrous carbonates and these minerals may be difficult to identify or distinguish from other hydrous minerals such as sulphates or chlorides.

Using IR to monitor stability and phase change kinetics

Amorphous $CaCO_3$ (ACC) is a thermodynamically unstable phase, and various parameters influence its transformation into $CaCO_3$ crystalline phases.[11] These parameters include

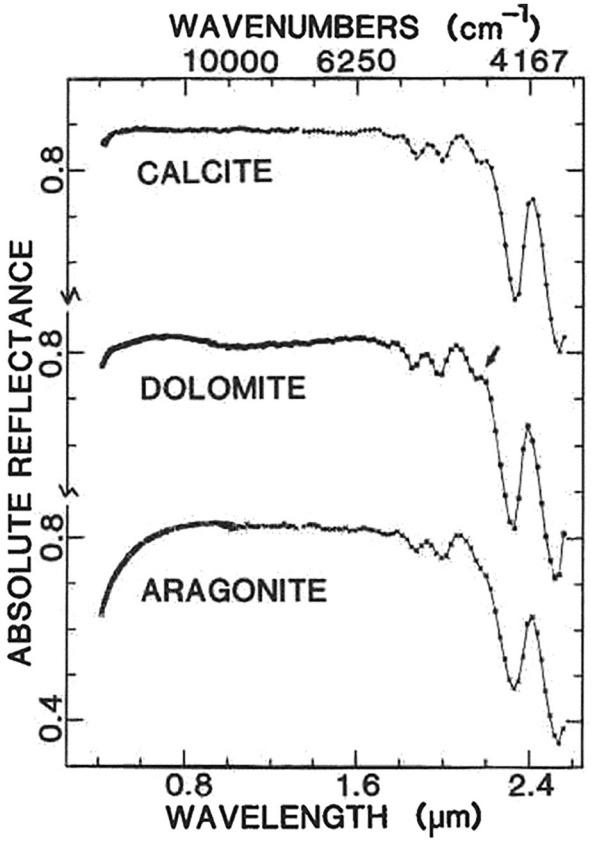

Fig. 3 Vis-NIR reflectance spectra of $CaCO_3$ minerals. Adapted from ref. 20 with permission from Mineralogical Society of America, copyright 1986.

impurities, pH and temperature. However, the amorphous phase can be stabilized at low particle sizes (<100 nm), using surfactants, or when contained in overbased (highly alkaline) detergent additives. An example is presented in Fig. 5 (ref. 23) where the amorphous phase was synthesized and stabilized by AOT (dioctyl sodium sulfosuccinate). However, heating to 70 °C, calcite and vaterite were obtained depending on the heating ramp. $CaCO_3$ polymorphs (including ACC) were also sometimes used as additives for lubricants and grease.[11]

ACC transformation into calcite (*via* thermal treatment and by exposure to water at RT) was monitored by IR, XRD and TGA.[24] Heating ACC resulted in the removal of adsorbed water above 100 °C with the formation of calcite at 270–400 °C. Similarly, exposure to a water/ethanol solution resulted in the crystallization of ACC. However, the product varied depending on the amount of water and the duration of exposure. Small water amount and/or short exposure time led to the formation of aragonite and/or vaterite, while more water and/or prolonged exposure led to the formation of calcite. The authors studied the influence of adding anionic polyelectrolytes, mimicking soluble proteins for inhibition of crystallization.

Similarly, the transformation of ACC to calcite was shown, using IR monitoring, to proceed *via* vaterite as a transition state.[25] A two-step mechanism was suggested starting with the formation of vaterite particles followed by a much slower step of redissolution and precipitation into calcite. Fig. 6 shows the XRD patterns corresponding to each step as well as the IR spectra of the initial and final materials.

IR was used to study naturally occurring spicules, skeletal elements in marine animals consisting of stable ACC entirely (in the ascidian Pyura pachydermatina) or of a composite of ACC and calcite (in the sponge Clathrina) (Fig. 7). In both cases, the presence of ACC was associated with proteins rich in glutamic acid (and/or glutamine), serine, glycine and polysaccharides,[26] while calcite was associated with proteins rich in aspartic acid (and/or asparagine).

Aragonite and vaterite transformation by heating into the more stable phase calcite was followed by IR spectroscopy.[19,27] The least stable phase vaterite was first prepared and its transformation into the other two phases was controlled. These transformations were clearly demonstrated by the significant changes in IR spectra at 650–1200 cm^{-1} (Fig. 8).

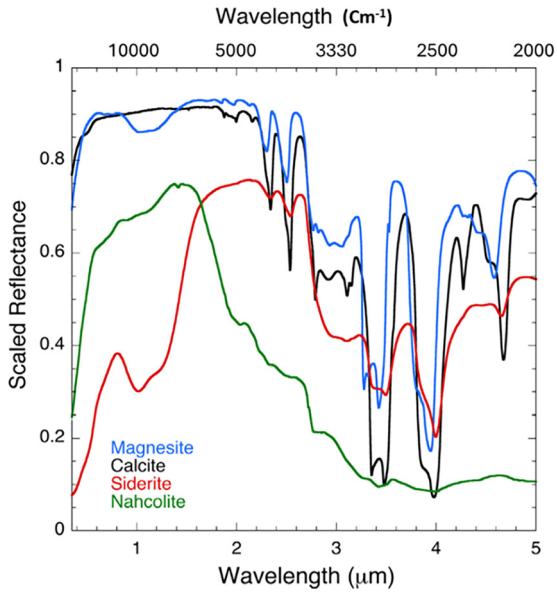

Fig. 4 NIR reflectance spectra (at 2000–28 571 cm^{-1}) of anhydrous carbonates: calcite, magnesite, siderite, and nahcolite. Adapted from ref. 21 with permission from Elsevier B. V., copyright 2015.

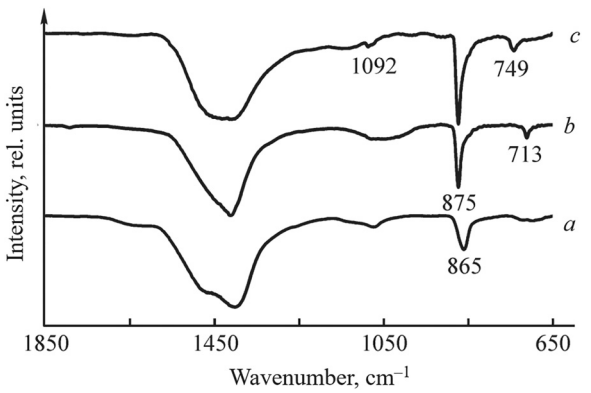

Fig. 5 IR spectra of (a) AOT-ACC, (b) calcite (heating ramp = 10 °C min^{-1}), and (c) vaterite (ramp = 1 °C min^{-1}). Adapted with permission from ref. 23 with permission from Royal Society of Chemistry, copyright 2013.

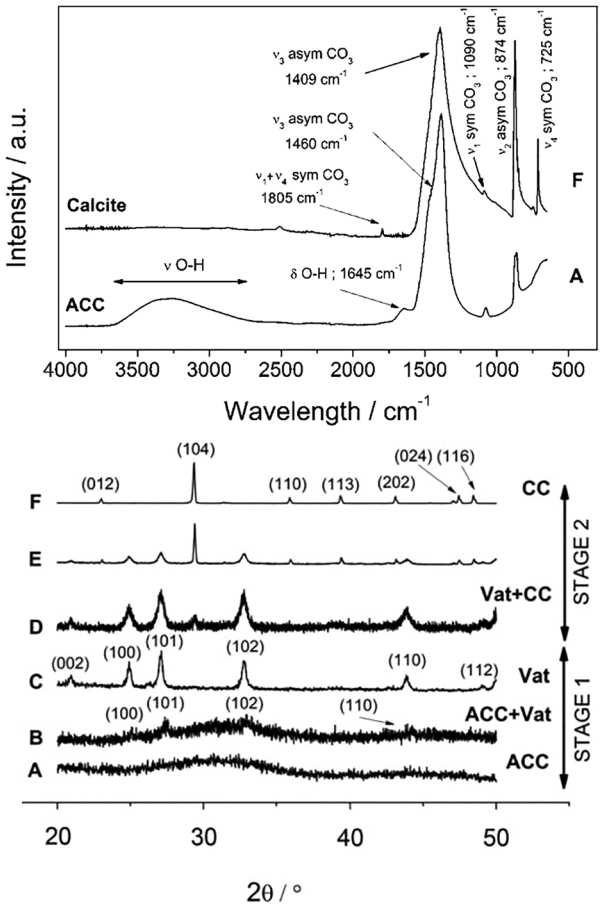

Fig. 6 Infrared spectra of ACC and calcite (top) showing the change in water content from the amorphous hydrated precursor to the non-hydrated crystalline calcium carbonate phases. 'A' and 'F' represent the same samples shown in the XRD patterns (bottom) of solids collected at different elapsed times during the off-line experiments, showing ACC, vaterite and calcite. Adapted from ref. 25 with permission from Royal Society of Chemistry, copyright 2011.

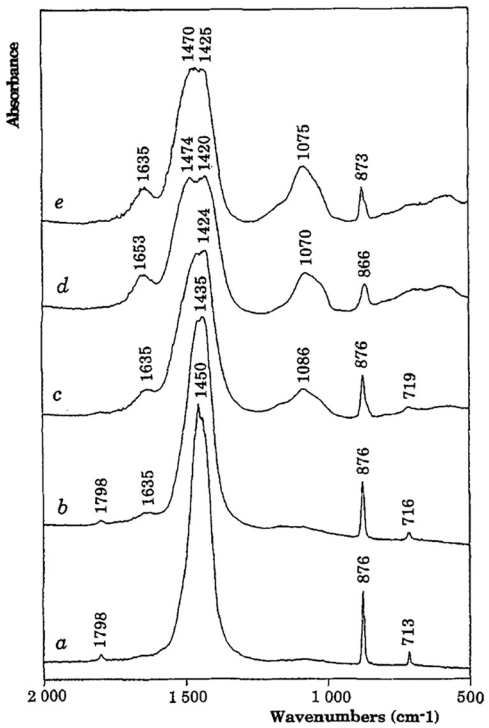

Fig. 7 IR spectra of calcium carbonates from (a) geological calcite, (b) separated calcitic cores from the Clathrina spicules, (c) intact Clathrina spicules (note the atypical broadening of the calcitic peaks and the additional absorption at 1080 cm^{-1}), (d) *P.pachydermaha* spicules, and (e) synthetic amorphous $CaCO_3$ grown in the presence of the macromolecules extracted from the amorphous layer of Clathrina spicules. Adapted from ref. 26 with permission from Wiley Online Library, copyright 1996.

Identification of carbonate composition: hydration of magnesium carbonate

The compositions and structure of several hydrous magnesium carbonates were studied using various techniques and IR spectroscopy which provided significant information.[28] Combining IR data published by several groups, a relationship was established between the infrared band frequencies and the lengths of H-bonds of various hydrated solids (including carbonates) (Fig. 9).[28] Moreover, Fig. 10 (ref. 28) shows FTIR spectra of three hydrated magnesium carbonate minerals where the bands due to structural hydrogen bonds varied significantly depending on the mineral structure.

IR studies of adsorbed species

The interaction of solid carbonates with small molecules and organic compounds is important for several concerns. Organic compounds govern the crystallization of biogenic carbonates in shells and marine organisms. In the field of oil extraction,

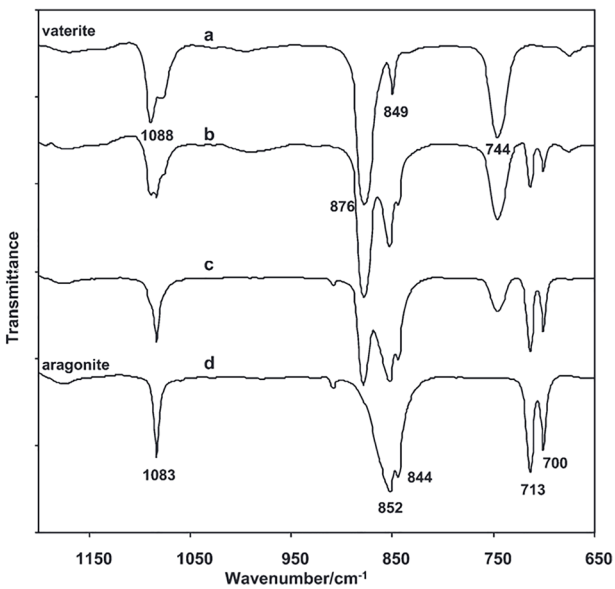

Fig. 8 FTIR spectra (650–1200 cm^{-1}) of (a) the vaterite sample, and when it was refluxed in distilled water for (b) 30 min, (c) 60 min, and (d) 75 min. Adapted from ref. 27 with permission from American Chemical Society, copyright 2010.

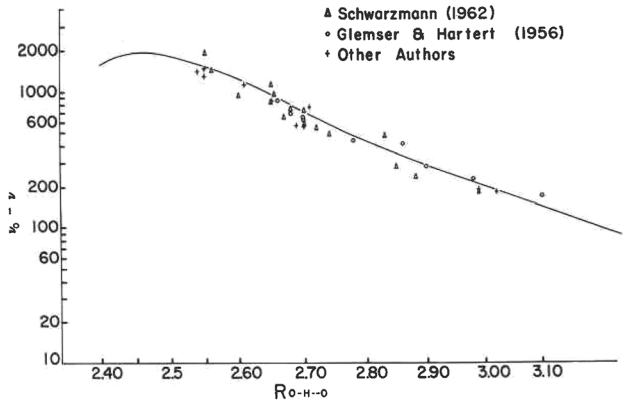

Fig. 9 Relationship between the O–H frequency (ν) and O–H···O distance in H-bonds ($R_{O-H\cdots O}$); where ν_0 = 3756 cm^{-1} on the *Y*-axis. Adapted from ref. 28 with permission from Mineralogical Society of America, copyright 1971.

understanding the way hydrocarbons and naphtha derivatives are adsorbed on carbonates is the key to extracting the maximum amount of oil from limestone deposits. Organics and probe molecules can also be adsorbed on the surface of solid carbonates for understanding surface sites on possible catalysts or on materials for sorption purposes.

Adsorption sites on carbonates

Adsorption sites vary depending on the type of molecule. Cationic metal sites are expected to be the preferential adsorption sites for most molecules such as CO,[1] H_2O[1] and HCs.[3–5] Carbonate groups, rather than the cations, are reported to be the preferential adsorption sites for CO_2.[2] Adsorbed water also leads to the formation of a surface intermediate $Ca(OH)HCO_3$[1,29,30] where SO_2 adsorbs on the hydrogen carbonate group, whereas CO_2 and inorganic acids adsorb on –OH groups.

Co-adsorption with water was found to strengthen CO adsorption on some solids and red-shift its absorption band[31] and similarly CO_2 adsorption on carbonate was enhanced due to adsorbed water.[29] Several adsorption models also explained the relationship between heats of adsorption, temperature and coverage. Temkin's model[32,33] suggests that heat of adsorption is inversely proportionally to coverage, and coverage is inversely proportional to temperature with a plateau of full coverage at relatively low temperatures.

Adsorption of CO

CO adsorbed on calcite yielded an IR absorption band at 2173–2176 cm^{-1} at a CO coverage of 2–0 L (Fig. 11). This indicates the rather weak adsorption, considering that gaseous CO absorption bands are located at 2114 and 2176 cm^{-1} (rotovibrational P and R branches, respectively). CO adsorption occurs over Ca cations.[34–36] Further infrared investigation of other carbonate minerals and different adsorption conditions is lacking.

The heat of adsorption and the vibrational spectrum were satisfactorily reproduced by DFT calculations for CO on calcite, with 2177 cm^{-1} (theoretically) for 2175 cm^{-1} (measured) at a coverage of 0.5 ML.[34]

Adsorption of CO_2

CO_2 methanation over Ni/dolomite was followed by *in situ* and *operando* DRIFTS and was found to proceed *via* CO_2 adsorption followed by the formation of formates, resulting finally in the formation of CH_4 and H_2O and not CO (Fig. 12-top).[37] Formates were observed after heating to 300 °C onwards as evidenced by

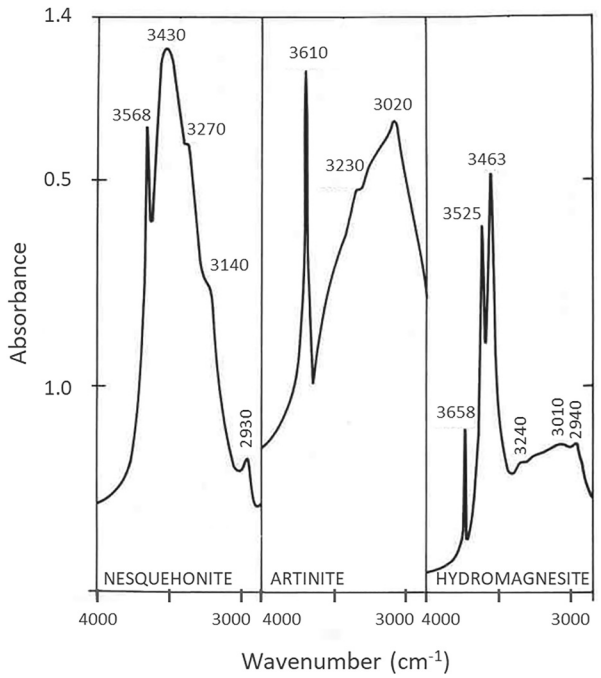

Fig. 10 Spectra of the hydrous magnesium carbonate minerals in the near infrared. Adapted from ref. 28 with permission from Mineralogical Society of America, copyright 1971.

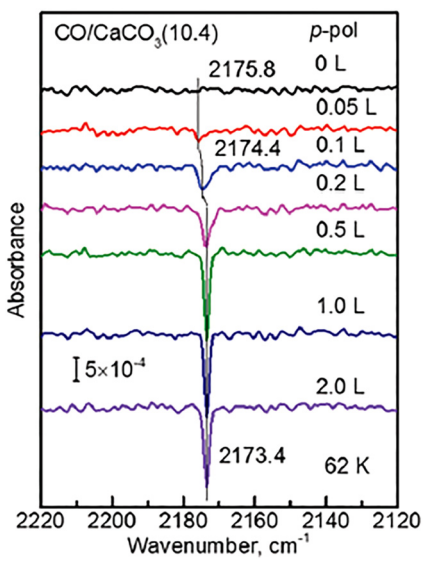

Fig. 11 IRRAS spectra with *p*-polarized light for CO adsorbed on the calcite (10.4) surface at 62 K with increasing exposures (0–2 L). Adapted from ref. 34 with permission from Royal Society of Chemistry, copyright 2021.

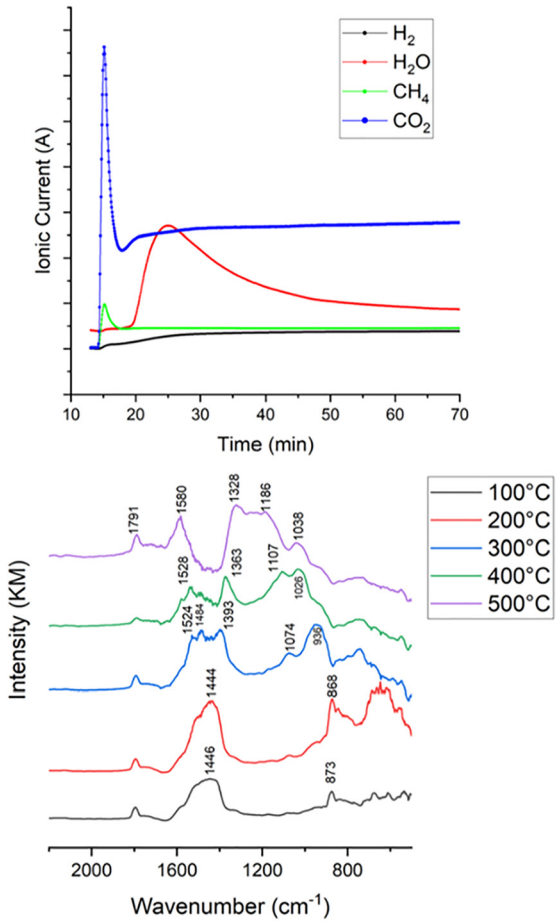

Fig. 12 Operando CO_2 methanation at 400 °C on Ni/dolomite: (Top) evolution of mass spectroscopy signal with reaction time. (Bottom) *In situ* DRIFT spectra as a function of catalyst temperature. Adapted from ref. 37 with permission from Elsevier B. V., copyright 2024.

the bands at 1393, 1484, 1524 cm^{-1} (Fig. 12 bottom). At 400 °C, a new band was detected at 1107 cm^{-1} and was ascribed to the formation of the methoxy group and an increased activity. At 500 °C, the intense carbonate $\nu 3$ band at ~1440 cm^{-1} disappeared due to thermal decomposition.

CO_2 was similarly found by FTIR to adsorb over hydrotalcite based catalysts during CO_2 methanation[38] or during surface activation by plasma glow discharge.[39] IR absorption bands of several carbonate species were detected upon introducing CO_2 over the hydrotalcite based catalyst (Fig. 13).

CO_2 adsorption was reported (without infrared data) to be positively affected by humidity, and H_2O leads to the formation of hydrogen carbonate species where CO_2 is adsorbed through –OH groups. Hydrogen carbonate was also formed during CO_2 adsorption over oxides depending on surface hydroxylation.[7]

CO_2 adsorption and reactivity were studied on several carbonate minerals and under different adsorption conditions including the presence of co-adsorbents. Adsorption sites and band positions were identified. Yet, FTIR studies are not abundant, and further works could bring about more insights.

As a matter of fact, CO_2 and CO adsorption represent a major carbon capture and storage (CCS) methodology which

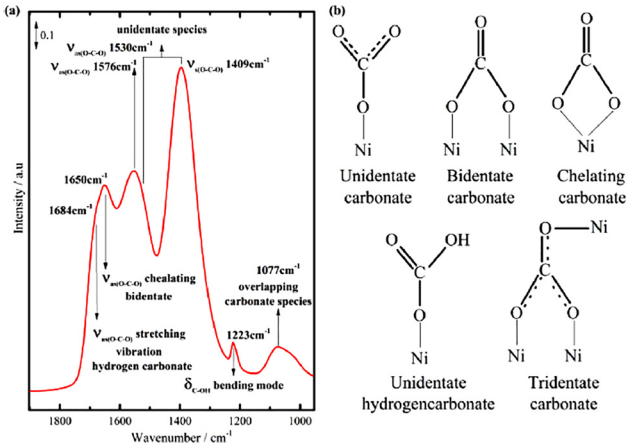

Fig. 13 (a) Infrared spectra of CO_2 adsorbed on the Ni-hydrotalcite derived catalyst and (b) possible species appeared in the CO_2 adsorption experiment. Adapted from ref. 38 with permission from Elsevier B. V., copyright 2023.

aims at reducing greenhouse gases in the atmosphere. Yet, this approach was sparingly followed by FTIR measurement in the literature reports despite its significance.

In this context, samples from naturally occurring carbonate reservoirs were reported to be efficient for CO_2 storage. For instance, CO_2-saturated brine was transported through the core sample and lead to changes in the permeability and porosity by creating conductive flow channels enhancing the rock's storage capacity.[40,41] Moreover, industrial projects were operated by applying CO_2 injections into carbonate rock reservoirs worldwide,[42,43] and indeed reported CO_2 storage efficiency.

On the other hand, over other CCS materials such as metal oxides,[7] Mg minerals[44] and cementitious materials,[45–47] upon adsorption of carbon oxides, carbonate formation was observed which in turn took part in further adsorption. Moreover, an electrochemical process was developed and efficiently capture CO_2 and form various carbonate salts[48] where the carbonate structure was evidenced by FTIR and XRD. This process represents a simulation of naturally occurring carbonate formation in sea water by the reaction of dissolved CO_2 with metal ions.

Adsorption of H_2O

Water adsorption on $CaCO_3$ forms a surface hydrogen carbonate species.[30] Consequently, CO_2 and HNO_3 are adsorbed through the –OH groups, whereas SO_2 is adsorbed *via* the hydrogen carbonate groups. This adsorption mechanism is consistent with a positive effect of H_2O on CO_2 adsorption on calcite.[29] In contrast, surface solvation (by H_2O) had a negative effect on the adsorption of aromatic hydrocarbons on calcite.[49] Fig. 14 (ref. 30) shows the evolution of ATR spectra of $CaCO_3$ during the exposure to a range of relative humidity. Increasing humidity induced an increased intensity for the IR bands due to adsorbed water around 1640 and 3000–3700 cm^{-1}.

Over hydrotalcites,[1] H_2O adsorption similarly leads to the formation of hydrogen carbonate and to the liberation of CO_2. This is accompanied by the formation of –OH groups detected

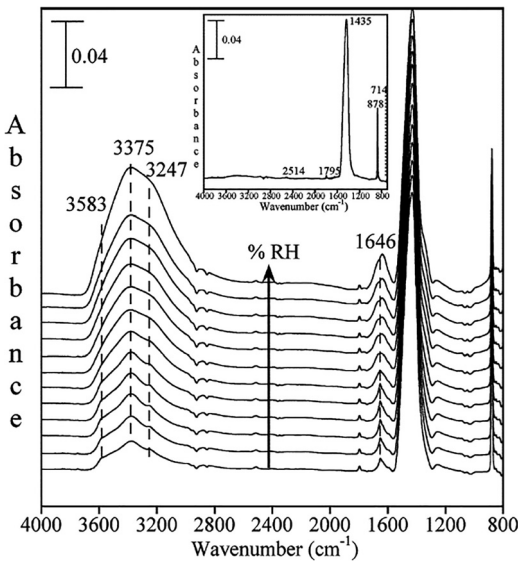

Fig. 14 Evolution of ATR-FTIR spectra during water adsorption on calcium carbonate as a function of relative humidity from 10.6 to 95.3% RH (10.6, 20.2, 29.8, 41.6, 50.1, 55.8, 60.1, 65.6, 70.7, 77.3, 81.5 and 95.3% RH). Inset: the ATR-FTIR spectrum of calcium carbonate under dry conditions (<5% RH). Adapted from ref. 30 with permission from Royal Society of Chemistry, copyright 2005.

by IR at 1490 and 3500 cm^{-1} (Fig. 15) and by the loss of carbonyl bond absorption bands at 1340 and 1570 cm^{-1}. Water is suggested to adsorb on cationic metal sites. The formation of hydrogen carbonates was also observed[29] as mentioned before.

Although there are few reports on H_2O adsorption on carbonates, valuable information is available about adsorption sites and reactivity. These works also demonstrated the positive effect of humidity on CO_2 adsorption and the negative effect of water on the adsorption of aromatic hydrocarbons.

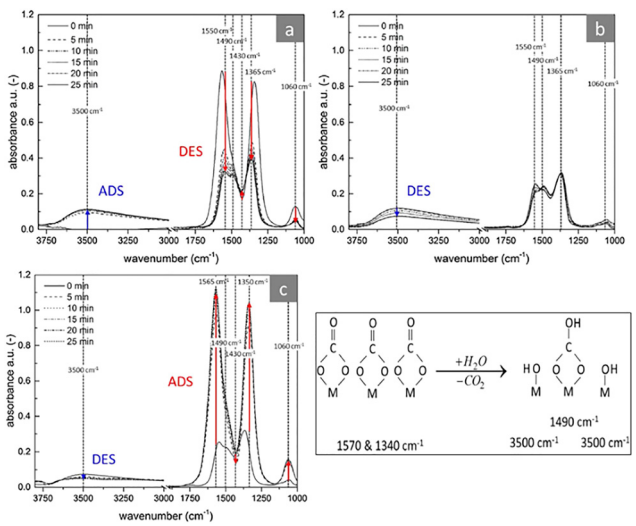

Fig. 15 IR spectra of hydrotalcite after (a) adsorption of H_2O at 400 °C, (b) desorption of H_2O at 400 °C with N_2 and (c) adsorption of CO_2 at 400 °C after desorption with H_2O and N_2. The equation shows H_2O adsorption and CO_2 liberation. Adapted from ref. 1 with permission from Elsevier B. V., copyright 2018.

Adsorption of hydrocarbons and functional molecules

The infrared spectrum of adsorbed probe molecules gives key information on surface sites and possible chemical reactions on the surface, for example with aromatics which are important for oil extraction purposes. Characteristic bands for the probe molecule are shifted upon adsorption, and more for the first monolayer than for the subsequent layers. An example of adsorbed benzene on calcite is shown in Fig. 16, where liquid benzene displayed a characteristic band at 667 cm^{-1} whereas it was shifted to 680 cm^{-1} in the case of a monolayer adsorbed on calcite and to 673 cm^{-1} in the case for extended adsorption layers.

Combining FTIR and DFT investigations proved useful to explain the interaction of calcite with four aromatic compounds.[51] Ionic bonds were formed as Ca–O (between calcite and benzoic acid, with the formation of –OH groups *via* oxygen atoms of calcite) and Ca–N (between calcite and pyridine). Thiophene was adsorbed *via* O–H bond formation, whereas toluene showed no interaction.

Combined MD and DFT computed a stronger CO_2 adsorption on $CaCO_3$ polymorphs compared to CH_4 adsorption,[2] in agreement with the previously mentioned observations.[52] Adsorption strengths of CH_4 and CO_2 were computed on vaterite, aragonite and calcite.[2]

Adsorption energies were also computed for benzene and hexane on calcite and dolomite[5] and Ca cations were suggested as the most energetically favorable adsorption sites. This is consistent with some experimental studies[4,52] but could easily be checked in detail with IR.

Tert-Butyl cyanide (TBC) was used as a probe for acidity on carbonated MgO (containing $MgCO_3$).[4] The cyanide group attached itself to Mg cations acts as weak Lewis acid sites. The ν(CN) absorption band is observed at 2234 cm^{-1} when TBC is only physisorbed, with no strong interaction. When the probe molecule is adsorbed on carbonate-free MgO, it is slightly shifted to 2240 cm^{-1}. On the carbonated solid, the stronger interaction leads to an upward shift to 2262 cm^{-1}, which indicates a stronger electron depletion on the cation because of the carbonate moiety (Fig. 17).

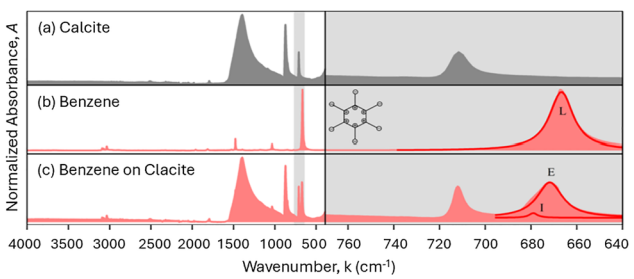

Fig. 16 [Left] IR spectra at 400–4000 cm^{-1} of (a) calcite, (b) benzene, and (c) benzene on calcite. [Right] Expanded view of 640–770 cm^{-1}. L: liquid, E: extended adsorption layers, I: first adsorption layer. Adapted from ref. 50 with permission from American Chemical Society, copyright 2015.

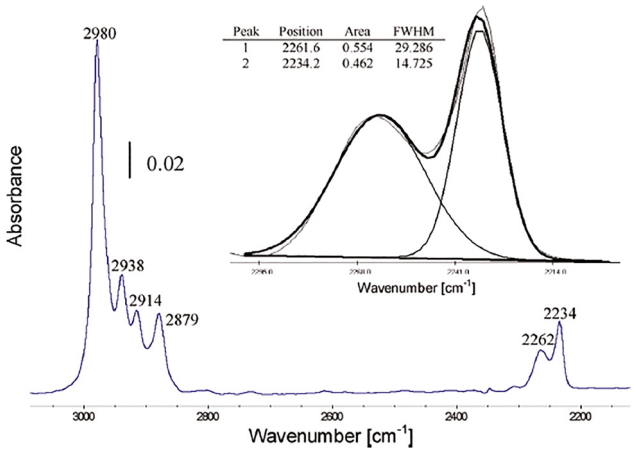

Fig. 17 *Tert*-Butyl cyanide adsorption on carbonated MgO activated at 240 °C. The zoom-in region of 2300–2150 cm^{-1}. The deconvolution results are shown in the inset. Adapted from ref. 4 with permission from American Chemical Society, copyright 2011.

CH_4 desorption and recovery from carbonate natural gas reservoirs were improved by hot CO_2 gas injections due to a favorable adsorption competition between CO_2 and methane[52] (Fig. 18). Detailed information on the molecular interactions by IR is, however, missing.

With aminoacids, experimental information is clearly missing. It was computed that anhydrous ACC favored the adsorption of basic/neutral aminoacids, whereas co-adsorbed water improved the adsorption of acidic aminoacids.[53] This study also suggested a faster diffusion of surface Ca^{2+} compared to the bulk ions. Experimental studies are needed to validate these findings.

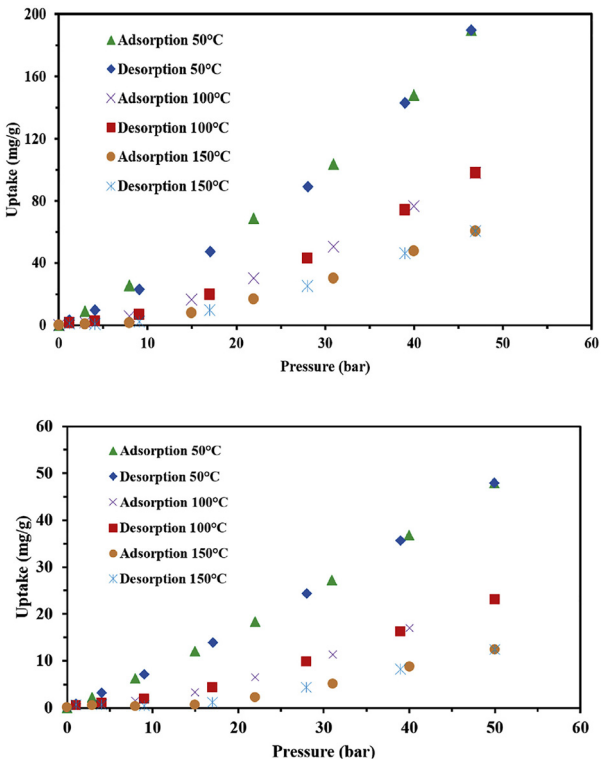

Fig. 18 Evolution with temperature and pressure of the adsorption and desorption of CO_2 (top) and CH_4 (below) on carbonate rocks. Adapted from ref. 52 with permission from Elsevier B. V., copyright 2018.

Conclusions

Infrared spectroscopy has proven to be a versatile, facile and inexpensive technique for studying carbonate minerals. FTIR techniques offer valuable information on their structural features, phase transitions, and on the remarkable adsorption capacities. This review builds up on the use of FTIR for studying the carbonate structure and the differentiation between its polymorphs, monitoring dehydration and rehydration processes, aiming at studying the adsorption mechanisms and adsorption sites for several molecules such as CO, CO_2, H_2O, and several HCs on carbonates. Some authors reported theoretical modeling and validated the results *via* experimental data, but FTIR remains underutilized in the literature for studying the surface properties of carbonates. Therefore, future works should target integrating FTIR (alongside computational modeling) to deepen our understanding of these surface properties including the nature of surface acidity. This, in turn, would be beneficial for several processes where carbonates are heavily involved such as CO_2 capture and storage and natural gas extraction.

Author contributions

All authors contributed to the conceptualization, bibliographic survey and design of the review. The original draft was written by Taha Elgayyar. Further modification and comments were performed by all authors. All authors approved of the final version of the review.

Conflicts of interest

There are no conflicts to declare.

Data availability

Our article represents a mini-review article, and all the figures included are adapted with permission from the corresponding references.

Acknowledgements

The authors are grateful to the region Normandie for financial aid (project ADSOCARB in the frame of the Normandie Emergent scheme).

References

1 K. Coenen, F. Gallucci, B. Mezari, E. Hensen and M. van Sint Annaland, *J. CO2 Util.*, 2018, **24**, 228–239.

2 M. Zhang, J. Li, J. Zhao, Y. Cui and X. Luo, *ACS Omega*, 2020, **5**, 11369–11377.
3 H. Wang, D. J. Grant, P. C. Burns and C. Na, *Langmuir*, 2015, **31**, 5820–5826.
4 J. Ni, F. C. Meunier, S. Robles-Manuel, J. Barrault and S. Valange, *J. Phys. Chem. C*, 2011, **115**, 24931–24936.
5 V. A. Rigo, C. O. Metin, Q. P. Nguyen and C. R. Miranda, *J. Phys. Chem. C*, 2012, **116**, 24538–24548.
6 S. Bordiga, C. Lamberti, F. Bonino, A. Travert and F. Thibault-Starzyk, *Chem. Soc. Rev.*, 2015, **44**, 7262–7341.
7 G. Busca and V. Lorenzelli, *Mater. Chem.*, 1982, **7**, 89–126.
8 G. Herzberg, *Molecular spectra and molecular structure. II, Infrared and Raman spectra of polyatomic molecules*, D. Van Nostrand Company, 1956.
9 G. C. Jones and B. Jackson, *Infrared Transmission Spectra of Carbonate Minerals*, 1993.
10 C. E. Weir and E. R. Lippincott, *J. Res. Natl. Bur. Stand. Sect. Phys. Chem.*, 1961, **65A**, 173.
11 V. N. Bakunin, D. R. Aleksanyan and Y. N. Bakunina, *Russ. J. Appl. Chem.*, 2022, **95**, 461–471.
12 R. C. H. Elderfield, *Am. Mineral.*, 1971, **56**, 1600–1606.
13 R. N. Clark, T. V. V. King, M. Klejwa, G. A. Swayze and N. Vergo, *J. Geophys. Res. Solid Earth*, 1990, **95**, 12653–12680.
14 E. Roedel, A. Urakawa, S. Kureti and A. Baiker, *Phys. Chem. Chem. Phys.*, 2008, **10**, 6190.
15 A. Bertoluzza, P. Monti, M. A. Morelli and M. A. Battaglia, *J. Mol. Struct.*, 1981, **73**, 19–29.
16 W. Sekkal and A. Zaoui, *Sci. Rep.*, 2013, **3**, 1–10.
17 L. Brečević and A. E. Nielsen, *J. Cryst. Growth*, 1989, **98**, 504–510.
18 F. A. Andersen and L. Brečević, *Acta Chem. Scand.*, 1991, **45**, 1018–1024.
19 J. Perić, M. Vučak, R. Krstulović, L. Brečević and D. Kralj, *Thermochim. Acta*, 1996, **277**, 175–186.
20 S. J. Gaffey, *Am. Mineral.*, 1986, **71**, 151–162.
21 P. L. Harner and M. S. Gilmore, *Icarus*, 2015, **250**, 204–214.
22 F. Khayamim, J. Wetterlind, H. Khademi, A. H. J. Robertson, A. F. Cano and B. Stenberg, *J. Infrared Spectrosc.*, 2015, **23**, 155–165.
23 E. H. Noel, Y.-Y. Kim, J. M. Charnock and F. C. Meldrum, *CrystEngComm*, 2013, **15**, 697–705.
24 X.-R. Xu, A.-H. Cai, R. Liu, H.-H. Pan, R.-K. Tang and K. Cho, *J. Cryst. Growth*, 2008, **310**, 3779–3787.
25 J. D. Rodriguez-Blanco, S. Shaw and L. G. Benning, *Nanoscale*, 2011, **3**, 265–271.
26 J. Aizenberg, L. Addadi, S. Weiner and G. Lambert, *Adv. Mater.*, 1996, **8**, 222–226.
27 A. Sarkar and S. Mahapatra, *Cryst. Growth Des.*, 2010, **10**, 2129–2135.
28 W. B. White, *Am. Mineral.*, 1971, **56**, 46–53.
29 C. Santschi and M. J. Rossi, *J. Phys. Chem. A*, 2006, **110**, 6789–6802.
30 H. A. Al-Hosney and V. H. Grassian, *Phys. Chem. Chem. Phys.*, 2005, **7**, 1266–1276.
31 S. D. Ebbesen, B. L. Mojet and L. Lefferts, *Phys. Chem. Chem. Phys.*, 2009, **11**, 641–649.
32 O. Dulaurent and D. Bianchi, *Appl. Catal., A*, 2000, **196**, 271–280.
33 O. Dulaurent, M. Nawdali, A. Bourane and D. Bianchi, *Appl. Catal., A*, 2000, **201**, 271–279.
34 T. M. Hafshejani, W. Wang, J. Heggemann, A. Nefedov, S. Heissler, Y. Wang, P. Rahe, P. Thissen and C. Wöll, *Phys. Chem. Chem. Phys.*, 2021, **23**, 7696–7702.
35 G. Blyholder, *J. Phys. Chem.*, 1964, **68**, 2772–2778.
36 J. Heggemann, Y. S. Ranawat, O. Krejčí, A. S. Foster and P. Rahe, *J. Phys. Chem. Lett.*, 2023, **14**, 1983–1989.
37 M. Canon-Alvarado, C. Blanco and C. Daza, *J. Environ. Chem. Eng.*, 2024, **12**, 112224.
38 M. Nguyen-Quang, F. Azzolina-Jury, F. Thibault-Starzyk, A. Travert, M. Ziąbka, B. Samojeden, M. Motak and P. Da Costa, *Appl. Mater. Today*, 2023, **32**, 1–15.
39 R. Dębek, D. Wierzbicki, M. Motak, M. E. Galvez, P. Da Costa and F. Azzolina-Jury, *Plasma Sci. Technol.*, 2019, **21**, 045503.
40 L. Luquot and P. Gouze, *Chem. Geol.*, 2009, **265**, 148–159.
41 Y. Yang, Y. Li, J. Yao, S. Iglauer, L. Luqot, K. Zhang, H. Sun, L. Zhang, W. Song and Z. Wang, *Water Resour. Res.*, 2020, **56**, 1–22.
42 M. Barbier, Y. Hamon, J.-P. Callot, M. Floquet and J.-M. Daniel, *Mar. Pet. Geol.*, 2012, **29**, 50–67.
43 D. Civile, M. Zecchin, E. Forlin, F. Donda, V. Volpi, B. Merson and S. Persoglia, *Int. J. Greenh. Gas Control*, 2013, **19**, 101–116.
44 H. S. Santos, H. Nguyen, F. Venâncio, D. Ramteke, R. Zevenhoven and P. Kinnunen, *Inorg. Chem. Front.*, 2023, **10**, 2507–2546.
45 A. Mahmood, A. Ibuk, M. Vogel, C. Neuhaus, F. Dehn and P. Thissen, *ACS Sustainable Chem. Eng.*, 2023, **11**, 13002–13012.
46 N. Giraudo and P. Thissen, *ACS Sustainable Chem. Eng.*, 2016, **4**, 3985–3994.
47 M. Izadifar, C. Natzeck, K. Emmerich, P. G. Weidler, S. Gohery, C. Burvill and P. Thissen, *J. Phys. Chem. C*, 2022, **126**, 12405–12412.
48 O. Oloye and A. P. O'Mullane, *ChemSusChem*, 2021, **14**, 1767–1775.
49 A. Budi, S. L. S. Stipp and M. P. Andersson, *Phys. Chem. Chem. Phys.*, 2018, **20**, 7140–7147.
50 H. Wang, D. J. Grant, P. C. Burns and C. Na, *Langmuir*, 2015, **31**, 5820–5826.
51 R. Chai, Y. Liu, Q. Liu and J. Xin, *Colloids Surf., A*, 2021, **612**, 1–13.
52 M. Eliebid, M. Mahmoud, R. Shawabkeh, S. Elkatatny and I. A. Hussein, *J. Nat. Gas Sci. Eng.*, 2018, **55**, 575–584.
53 R. Innocenti Malini, A. R. Finney, S. A. Hall, C. L. Freeman and J. H. Harding, *Cryst. Growth Des.*, 2017, **17**, 5811–5822.